Banner appropriate to article type will appear here in typeset article

Subgrid Stress Modelling with Multi-dimensional State Space Sequence Models

Andy Wu¹† and Sanjiva K. Lele^{1, 2}

(Received xx; revised xx; accepted xx)

Large Eddy Simulations (LES) are becoming increasingly viable due to the growth in computational power the last few decades, and subgrid stress modelling plays a large role in the accuracy of LES. A new class of neural network models, S4 and S4ND models, allow for learning a continuous representation of the discrete dataset, which facilitates a principled approach to incorporating grid dependence in neural network subgrid stress modelling. A S4ND Unet neural network architecture is proposed and trained on both forced Homogeneous Isotropic Turbulence (HIT) and channel flow, where *a priori*, it is shown to generalize to grid spacings that are coarser than the training set grid spacings, while simpler artificial neural network (ANN) models fail. *A posteriori* tests on both forced HIT and channel flow indicate that the S4ND model is more accurate than traditional models and ANN-based models on grid sizes that are in the training set. The S4ND model is also able to generalize to grid sizes that are coarser than the training set *a posteriori*, and is more accurate than many traditional and neural network subgrid stress models. Finally, the proposed model is also evaluated on flows at increasing Reynolds numbers, where it is seen that the proposed neural network remains stable even at a Reynolds number that is 500,000 times that seen in the training set.

Key words: Authors should not enter keywords on the manuscript, as these must be chosen by the author during the online submission process and will then be added during the typesetting process (see Keyword PDF for the full list). Other classifications will be added at the same time.

MSC Codes (Optional) Please enter your MSC Codes here

1. Introduction

Large Eddy Simulations (LES) provide an efficient paradigm to economically simulate turbulent flows and potentially flows of engineering interest by simulating the large scale, predominantly energy containing turbulent eddies while modelling the small scale turbulent

† Email address for correspondence: awu1018@stanford.edu

¹Department of Aeronautics and Astronautics, Stanford University, Stanford, California, USA

²Department of Mechanical Engineering, Stanford University, Stanford, California, USA

structures (Goc *et al.* 2021). Thus, in order to close the governing equations, subgrid-scale (SGS) modelling, the act of modelling the effect of small scale turbulent structures, is employed. SGS modelling has a significant impact on the accuracy and stability of LES (Pope 2000; Sagaut 2006). In general, SGS models can be split into two major categories, models being driven by statistical approximations inspired by turbulence theory, or derived from data (with additional constraints that may or may not be driven by turbulence theory). In each of these two major categories, one can additionally make the characterization of the model being functional, structural, or a mix of both (Prakash *et al.* 2022; Sagaut 2006). Functional models aim to approximate the effect of smaller-scale structures of turbulence on the larger scales, contributing to the stability of the LES simulation (Sagaut 2006). Oftentimes, these models do not have high correlation with the subgrid stress tensor, τ_{ij} . Meanwhile, structural models aim to capture the the subgrid stress tensor more accurately, but often do not capture the true energy dissipation associated with the small scales, and can be destabilizing to LES (Sagaut 2006).

Traditionally, SGS models are statistical approximations inspired by turbulence theory, whether they are functional or structural. One of the first SGS models for LES, the Static Smagorinsky model (Smagorinsky 1963), assumes a perfect alignment between the resolved rate of strain tensor, \bar{S}_{ij} and τ_{ij} (Pope 2000). Both the Static Smagorinsky and Dynamic Smagorinsky models (Germano et al. 1991) are based on inertial range energetics, where the rate of energy transfer from large scale to small scale structures is equivalent to the viscous dissipation at small scales. Other models, such as the Sigma model (Nicoud et al. 2011), compute the eddy-viscosity coefficient differently as compared to the Static and Dynamic Smagorinsky models to incorporate more turbulence theory (subgrid stress must vanish in laminar flows), but are still rooted in the same theory of inertial range energetics (Vreman 2004). The Sigma model represents a significant advance in traditional subgrid stress modelling, as by using the singular values of the resolved velocity gradient tensor, the model predicts zero subgrid stress if the resolved field is two-dimensional or two-component, vanishes in laminar flow, and has cubic behavior at the wall (Nicoud et al. 2011). Even then, all the models listed thus far have been functional models. A different subset of models, structural models, do not focus on the energy dissipation and instead are predicated on capturing higher correlation with the subgrid stress tensor. For example, Clark's Gradient model (Clark et al. 1979) for the subgrid stress tensor is derived from a Taylor series expansion assuming an isotropic filter. The Scale-Similarity Model (Bardina 1983; Berselli et al. 2006), assumes inertial range scale-similarity, suggesting that the subgrid stress tensor can be inferred from doubly-filtered and filtered velocities. Since these models do not incorporate insights associated with turbulence energetics explicitly, often, they are destabilizing to a LES, even if the predicted subgrid stress tensor has higher correlation to the actual subgrid stress tensor (Prakash et al. 2022; Beck & Kurz 2021).

Recently, with the advance of deep learning and the availability of high quality Direct Numerical Simulation (DNS) data online, learning a closure to the governing equations has become tractable instead of approaching subgrid stress modelling from a purely theoretical perspective (Park & Choi 2021; Beck *et al.* 2019; Stoffer *et al.* 2021; Maejimam & Kawai 2024; Xie *et al.* 2020a). Some of the early work done using machine learning involved using the velocity gradient and stresses to predict an eddy-viscosity coefficent (Sarghini *et al.* 2003). Models along this line of thought can be considered data-driven functional models. Another approach involves predicting the subgrid forcing term using neural networks, which directly approximates the term seen in the governing equations, or directly approximating τ_{ij} (Xie *et al.* 2020a,b). How τ_{ij} or the divergence of τ_{ij} is found varies, as Yuan *et al.* (2020) and Stolz *et al.* (2001) adopt a deconvolution approach, while others such as Xie *et al.* (2020a) use a tensor basis neural network (TBNN) with associated invariants as inputs (Wu

& Lele 2025). Others use the velocity gradient tensor as an input to a neural network to predict τ_{ij} (Park & Choi 2021; Kang *et al.* 2023), or incorporate second derivatives into the neural network input (Pawar *et al.* 2020; Wang *et al.* 2018). Another approach is to use mixed-models, where functional and structural models are mixed together to form one model, with the neural network learning the balance between the functional and structural models (Beck *et al.* 2019; Prakash *et al.* 2022). One can also adopt a reinforcement learning approach, where the neural network is given feedback at every "simulation timestep" and learns according to a reward function (Kurz *et al.* 2023; Bae & Koumoutsakos 2022). In the end, all these methods are just a way to either learn an eddy viscosity coefficient (functional), some part of the subgrid stress tensor (structural), or a mix of both.

Despite all this progress, neural network models are still not as flexible as traditional models, and the above works have all mainly focused on grid sizes that are relatively fine (only 4-8 times that of the DNS grid spacing, at most 16 times). Furthermore, it is well known that neural network models have trouble generalizing to grid spacings that are coarser than the training data (Cho et al. 2024; Kang et al. 2023). As such, Cho et al. (2024) adopt a recursive approach, where a neural network is continually augmented with higher Reynolds Number (Re) data trained on LES integrated with a neural network subgrid stress model. This approach is able to generalize to a wide range of Reynolds Numbers and grid spacing, and is one of the few investigations at a coarse LES grid spacing (when compared to the DNS grid spacing). Predominantly, neural network subgrid stress modelling only uses simple architectures such as Artifical Neural Networks (ANNs) (Kang et al. 2023; Park & Choi 2021; Cho et al. 2024; Stoffer et al. 2021; Xie et al. 2020a,b; Yuan et al. 2020, 2021; Sarghini et al. 2003; Sirignano & MacArt 2023; Cheng et al. 2022) or simple Convolutional Neural Networks (CNNs) (Guan et al. 2022; Beck et al. 2019). Given the advance of deep learning, it stands to reason that using more advanced neural network architectures could gain the generalization capability necessary for neural network models to be more flexible. As seen, Wu & Lele (2025) use a two neural network Convolutional Unet architecture trained on both channel flow and forced Homogeneous Isotropic Turbulence (forced HIT), showing that it improves upon traditional models and machine learning (ML) models using more simple architectures at larger grid spacings (LES grid spacings that are 16 and 32 times the DNS grid spacing). However, generalization to coarser grid spacings than the training set is still lacking.

In deep learning, a new class of models that have been gaining traction involve learning continuous convolution kernels (Li *et al.* 2021; Nguyen *et al.* 2022). Since typical convolutional neural network architectures are discrete, they are not sensitized to the grid spacing. Therefore, it is not surprising that they are unable to generalize to coarser grid spacings for subgrid stress modelling. However, continuous convolution kernels explicitly account for the grid spacing, potentially allowing for generalization to coarser grid spacing than the training data. One class of models from the computer vision community, the S4ND model (Nguyen *et al.* 2022), allows for continuous convolution kernels to be learned by parameterizing each spatial dimension with a State Space Model (Gu *et al.* 2021). By using the S4ND model in place of traditional convolutions, while enforcing the subgrid stress tensor symmetries through a Tensor Basis Neural Network (TBNN), a new neural network for subgrid stress modelling is created.

The main contributions of this paper include introducing a new neural network architecture that can generalize to coarser grid spacings not seen during training without any additional re-training, first in an *a priori* setting. This paper also contributes *a posteriori* analysis of the neural network. After the neural network is trained on both forced HIT and channel flow data, it is integrated into LES simulations of both forced HIT and channel flow, where it also successfully generalizes to a coarser grid spacing unseen during training while being more

accurate than traditional and other data-driven SGS models. Further analysis also shows that the neural network model can generalize to *Re* up to 500 times the *Re* in the training set, while also extrapolating in grid spacing without the need to train on any additional LES data or undergo transfer learning. This neural network subgrid stress model is also able to remain stable even when the *Re* is over 500,000 times larger than what it was trained on.

2. Numerical and Neural Network Details

This section provides background on the LES framework used, as well as the neural network model and training details.

2.1. LES Governing Equations

The governing LES equations solved are the filtered incompressible Navier Stokes Equations. The filtering operation is defined below:

$$\bar{\chi}(\mathbf{x},t) = \int G(\mathbf{r})\chi(\mathbf{x} - \mathbf{r},t)dr$$
 (2.1)

$$\int G(\mathbf{r})dr = 1 \tag{2.2}$$

where χ is the flow variable to be filtered, $G(\mathbf{r})$ is the filtering kernel, and $\bar{\chi}$ is the filtered flow variable. In all sections, the overbar operator is used to denote filtered quantities.

Now that the filter is defined, the governing equations are written below (in Einstein's summation notation):

$$\frac{\partial \bar{u}_i}{\partial x_i} = 0$$

$$\frac{\partial \bar{u}_i}{\partial t} + \bar{u}_j \frac{\partial \bar{u}_i}{\partial x_j} = -\frac{1}{\rho} \frac{\partial \bar{p}}{\partial x_i} + \nu \frac{\partial^2 \bar{u}_i}{\partial x_j \partial x_j} - \frac{\partial \tau_{ij}}{\partial x_j}$$

$$\tau_{ij} = \overline{u_i u_j} - \bar{u}_i \bar{u}_j$$
(2.3)

where \overline{p} is the filtered pressure, ρ is the density, \overline{u} is the filtered velocity, and v is the kinematic viscosity. The velocity field is solenoidal as seen from the continuity equation, and filtering the momentum equation results in obtaining the unclosed term, τ_{ij} . This tensor is computed by obtaining the filtered nonlinear product of the velocities before filtering, and then subtracting by the product of the filtered velocities. In LES only the filtered values of the dependent variables are available, thus, τ_{ij} can't be computed and has to be modelled. In the present work, all simulations are in the incompressible regime, and the neural network will learn to approximate τ_{ij} directly.

2.2. State Space Models and S4ND

Recently, a new class of models, structured state space sequence (S4) models has emerged from the natural language processing community (Gu *et al.* 2021). For a 1 dimensional problem, the neural network attempts to learn a state space representation:

$$\dot{\mathbf{x}} = \mathbf{A}\mathbf{x} + \mathbf{B}\mathbf{u}$$

$$\mathbf{y} = \mathbf{C}\mathbf{x} + \mathbf{D}\mathbf{u}$$
(2.4)

where **A**, **B**, **C**, **D**, are learnable matrices, **u** represents a 1D input (function of time), **x** represents the state vector (dimension of this state vector is specified by the user), while

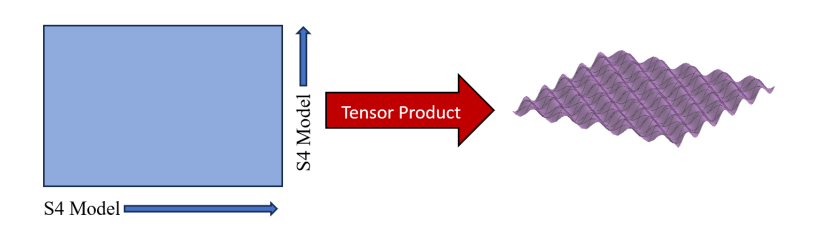


Figure 1: S4ND extension of the S4 model. A S4 model is instantiated in each direction, and then an outer product is taken to produce a continuous convolution kernel. When training and during inference, the continuous convolution kernel is discretized.

y represents the output vector. In general, **D** is ommitted as it can be viewed as a skip connection, which can be added in the neural network architecture (Gu *et al.* 2021). As seen, the neural network learns an underlying continuous representation from the discrete data. However, since the data is discrete, there needs to be a connection between the continuous and discrete setting. This connection is derived for the bilinear method (Gu *et al.* 2021). One can write the discretized state space as (the tilde operation signifies the discretized matrices):

$$\mathbf{x}_{k} = \tilde{\mathbf{A}}\mathbf{x}_{k-1} + \tilde{\mathbf{B}}\mathbf{u}_{k}$$

$$\mathbf{y}_{k} = \tilde{\mathbf{C}}\mathbf{x}_{k}$$

$$\tilde{\mathbf{A}} = (\mathbf{I} - \frac{\Delta}{2} \cdot \mathbf{A})^{-1}(\mathbf{I} + \frac{\Delta}{2} \cdot \mathbf{A})$$

$$\tilde{\mathbf{B}} = (\mathbf{I} - \frac{\Delta}{2} \cdot \mathbf{A})^{-1}\Delta\mathbf{B}$$

$$\tilde{\mathbf{C}} = \mathbf{C}$$
(2.5)

As seen, when discrete values (such as during training) are needed since the training data is discrete, the state space can be discretized with a spacing parameter Δ and a discretization method such as the bilinear method or zero order hold (Gu *et al.* 2021). This ensures that the neural network, while learning from discrete data, has an underlying continuous representation, which is enabled by the additional knowledge of the spacing parameter Δ . The underlying continuous representation it learns can be found by writing the non-tilde matrices as a function of the tilde matrices. By learning this underlying continuous representation and then being able to discretize using a specified grid spacing, the S4 model has been found to generalize very well to different Δ not in the training set (Gu *et al.* 2021).

This approach was extended to problems involving two dimensions in the computer vision community with the introduction of the S4ND model (Nguyen *et al.* 2022). The core idea behind the S4ND model, illustrated in figure 1, is to learn global, continuous convolution kernels by initializing a S4 model in each spatial dimension, and then taking the tensor outer product in order to obtain a continuous convolution kernel. Now, the Δ spacing parameter is the grid spacing. In other words, $\Delta = \Delta_g$ where Δ_g denotes the spatial spacing. When convolving the continuous convolution kernel with the discrete data, the spatial spacing is used to discretize the convolution kernel into a discrete convolution kernel before applying the convolution operation. Thus, the S4ND model can be used to replace traditional convolutions as a grid spacing aware operator, while traditional convolutions are agnostic to grid spacing. Overall, the S4ND model allows the neural network to learn continuous multi-dimensional representations of the data, which is more in line with fluid dynamics (continuum approximation), as the governing equations are continuous and then discretized onto a grid for LES.

In addition, since the state space is now discretized with a specific spatial spacing Δ_g , S4ND introduces a novel idea called bandlimiting (Nguyen et~al.~2022), which seeks to remove spurious frequencies in the convolution kernel that can't be supported by the grid spacing implied by Δ_g . If **A** is diagonal, then the state space convolution kernel "basis" can be represented by $e^{a_n t} B_n$, where a_n denotes the nth diagonal element of **A**. Therefore, a_n is a parameter that controls the frequency of the basis function associated with the convolution kernel. In order to mask out spurious frequencies in the convolution kernel, S4ND introduces a bandlimiting parameter, α , which is a hyperparmeter. If $a_n \Delta_g > \frac{1}{2}\alpha$, then this convolution kernel basis function is masked out, as this means that the frequency of the basis function is larger than what the grid can support (it is spurious). When $\alpha = 1$, bandlimiting corresponds to masking out everything above the Nyquist wavenumber. However, due to the finite state representation and also the decay associated with the real part of a_n , α is set lower empirically (between 0.1 and 0.6), which creates smoother convolution kernels (Nguyen et~al.~2022). In this work, $\alpha = 0.1$ is used.

2.3. Neural Network Architecture

The neural network involves replacing discrete convolutions with the S4ND block in a U-net architecture, followed by a backend tensor basis neural network (TBNN).

2.3.1. Tensor Basis Neural Network

The TBNN, originally introduced by Ling *et al.* (2016), involves computing the invariants and the tensor basis assuming that the subgrid stress tensor is a function of the resolved rate of strain tensor, $\bar{\mathbf{S}}_{ij}$, and the resolved rotation rate tensor, $\bar{\mathbf{R}}_{ij}$. A detailed derivation of the tensor basis and invariants for the subgrid stress tensor can be found in works such as Stallcup *et al.* (2022) and Wu & Lele (2025). Below, the invariants and tensor basis are listed for reference.

If one assumes that:

$$\tau_{ij} = F(\bar{\mathbf{S}}_{ij}, \bar{\mathbf{R}}_{ij}) \tag{2.6}$$

$$\bar{\mathbf{S}} \equiv \bar{\mathbf{S}}_{ij} = \frac{1}{2} \left(\frac{\partial \bar{u}_i}{\partial x_j} + \frac{\partial \bar{u}_j}{\partial x_i} \right) \tag{2.7}$$

$$\mathbf{\bar{R}} \equiv \mathbf{\bar{R}}_{ij} = \frac{1}{2} \left(\frac{\partial \bar{u}_i}{\partial x_j} - \frac{\partial \bar{u}_j}{\partial x_i} \right) \tag{2.8}$$

then the invariants can be written as:

$$\{tr(\bar{\mathbf{S}}), tr(\bar{\mathbf{S}}^2), tr(\bar{\mathbf{S}}^3), tr(\bar{\mathbf{R}}^2), tr(\bar{\mathbf{S}}\bar{\mathbf{R}}^2), tr(\bar{\mathbf{S}}^2\bar{\mathbf{R}}^2), tr(\bar{\mathbf{S}}^2\bar{\mathbf{R}}^2\bar{\mathbf{S}}\bar{\mathbf{R}})\}$$
(2.9)

and the tensor basis can be written as:

$$\{I, \bar{S}, \bar{S}^2, \bar{R}^2, \bar{S}\bar{R} - \bar{R}\bar{S}, \bar{R}\bar{S}\bar{R}, \bar{S}^2\bar{R} - \bar{R}\bar{S}^2, \bar{R}\bar{S}\bar{R}^2 - \bar{R}^2\bar{S}\bar{R}\}$$
(2.10)

As seen, the invariants involve extremely high powers of the resolved strain rate and rotation rate tensors, which are not ideal due to aliasing errors, which increase with increasing power (Roberts & Mullis 1987). Thus, instead of using the invariants, which are mathematically complete, one can simply use the velocity gradient tensor in place of the invariants, which is an input commonly used for neural network subgrid stress models (Park & Choi 2021; Kang *et al.* 2023; Cho *et al.* 2024). It is noted that there is no performance degradation using the velocity gradient tensor instead of the invariants as inputs to the neural network. Even if the input to the neural network is changed, the backend of the neural network remains the same. The neural network will predict coefficients of the tensor basis expansion, listed here as $c_1 - c_8$ (8 scalar values are predicted given the filtered velocity gradient tensor

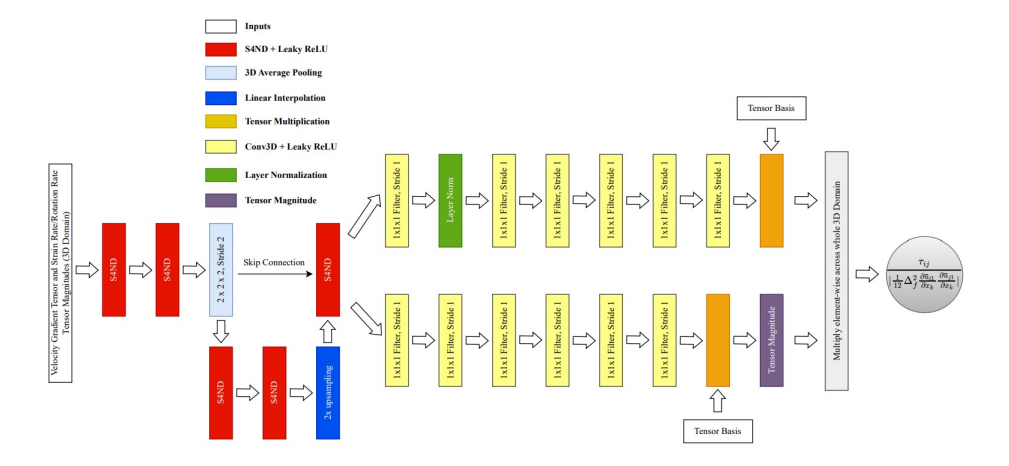


Figure 2: The overall neural network architecture. The whole 3D domain is inputted into the neural network, and the output is the corresponding subgrid stress at each point. For each S4ND layer, a state space dimension of 8 was chosen to keep the trainable parameters comparable to existing models in literature. The average pooling operation will downsample all spatial dimensions by a factor of 2. As seen, after the final S4ND layer, the neural network architecture splits into two "prediction heads" to predict the "magnitude" and "structure" of the subgrid stress tensor, and both prediction heads use the tensor basis (each prediction head predicts its own set of coefficients to multiply the tensor basis components). See Wu (2025) for downloadable version of the model and an example input/output.

as an input):

$$\tau_{ij} = c_1 \mathbf{I} + c_2 \bar{\mathbf{S}} + c_3 \bar{\mathbf{S}}^2 + c_4 \bar{\mathbf{R}}^2 + c_5 (\bar{\mathbf{S}}\bar{\mathbf{R}} - \bar{\mathbf{R}}\bar{\mathbf{S}}) + c_6 \bar{\mathbf{R}}\bar{\mathbf{S}}\bar{\mathbf{R}} + c_7 (\bar{\mathbf{S}}^2\bar{\mathbf{R}} - \bar{\mathbf{R}}\bar{\mathbf{S}}^2) + c_8 (\bar{\mathbf{R}}\bar{\mathbf{S}}\bar{\mathbf{R}}^2 - \bar{\mathbf{R}}^2\bar{\mathbf{S}}\bar{\mathbf{R}})$$
(2.11)

2.3.2. Overall Architecture

Now that the backend TBNN is introduced, the overall neural network architecture can be seen in figure 2. The inputs to the neural network are the three dimensional, spatially varying velocity gradient tensor, as well as the strain rate and rotation rate tensor magnitudes. These inputs are passed into a U-net S4ND architecture that allows for multiscale fusion of different spatial scales of turbulence. After the U-net architecture, the neural network splits into two streams. Wu & Lele (2025) found that using two neural networks, one to predict the magnitude of τ_{ij} while the other predicts the structure (normalized) τ_{ij} results in better performance. This neural network architecture retains the idea of predicting a "structure" component and a "magnitude" component, but is able to do it in one single neural network instead of splitting the task of predicting a "structure" or "magnitude" component to separate neural networks. As seen, the neural network splits into two paths after the U-net architecture, with both paths using the tensor basis neural network (predicting 8 coefficients that multiply the tensor basis). However, instead of using fully connected layers, which are unable to handle different domain sizes, 1x1x1 convolutions are used, which can emulate fully connected layers while still being able to generalize to various domain sizes.

Non-dimensionalizing the model and scaling the inputs and outputs are crucial to training a neural network model. Here, the inputs (velocity gradient tensor, strain rate and rotation rate tensor magnitudes, so a total of 11 quantities at each point in the domain) are normalized

with a max-min scaling:

$$x_{norm} = \frac{x - x_{min}}{x_{max} - x_{min}} * 2 - 1 \tag{2.12}$$

where *x* corresponds to every component of the velocity gradient tensor (or the strain rate/rotation rate tensor magnitudes). The maximum and minimum correspond to the 3D domain's maximum and minimum. This input normalization ensures that the neural network model inputs are always scaled between [-1, 1]. The tensor basis are also scaled, although with the Frobenius Norm instead:

$$W_{ij}^{norm} = \frac{W_{ij}}{|W_{ij}|} \tag{2.13}$$

where W_{ij} is a tensor corresponding to a tensor in the tensor basis expansion. Note that in Equation 2.13, repeated indices do not imply summation. Furthermore, the output is also normalized accordingly to ensure that the model is non-dimensional. Following observations made by Kang *et al.* (2023), the Clark's gradient model term is taken as a normalization for τ_{ij} , as seen in figure 2. However, one small modification is made. Work done by Scotti *et al.* (1993) introduced the anisotropic mesh length factor, f, which multiplies the effective grid width Δ_e as grid anisotropy may play a role in determining τ_{ij} . Therefore, the normalization used for τ_{ij} becomes:

$$\frac{\tau_{ij}}{\left|\frac{1}{12}\Delta_f^2 \frac{\partial \bar{u}_l}{\partial x_k} \frac{\partial \bar{u}_m}{\partial x_k}\right|} \tag{2.14}$$

where $\Delta_f = f\Delta_e$, $f = 1 + \frac{2}{27}[ln(a_1)^2 - ln(a_1)ln(a_2) + ln(a_2)^2]$ and $\Delta_e = (\Delta_1\Delta_2\Delta_3)^{\frac{1}{3}}$. Δ_i denotes the grid spacing in the ith dimension, while a_1 and a_2 denote the grid spacing ratios (both less than 1).

2.4. Neural Network Training Details

This section goes over the process of querying the training data, as well as introducing the loss function and some metrics that can be used to quantify the performance of the neural networks in a LES *a posteriori*.

2.4.1. Training Data

Both filtered HIT and channel flow data are queried from the Johns Hopkins Turbulence Database (JHTDB), a service that provides high-quality DNS data for research purposes (Li et al. 2008; Perlman et al. 2007; Graham et al. 2016). From Park & Choi (2021), training on two different filter widths provides the neural network with more generalizability to different grid spacings. Thus, since this paper is focused on applications to aggressive, coarse grid spacing settings, after quering the DNS data, the DNS data is filtered to a filter width corresponding to $\Delta_g = 16\Delta_{DNS}$ and $\Delta_g = 32\Delta_{DNS}$, where Δ_{DNS} denotes the DNS grid spacing. The filtering operation involves using a box filter in physical space. Following Wu & Lele (2025), two different domain sizes are also queried in order to help the neural network generalize to various domain sizes. The querying procedure used here is identical to that used in Wu & Lele (2025). In total, the training data contents are listed in Table 1.

The training data is divided into 80 percent for training, 10 percent for validation, and 10 percent as a held-out test set. Each of the categories above is split according to the percentages above and then recombined into the total training, total validation, and total test set. In addition, filter width $\Delta_g = 24\Delta_{DNS}$ and filter width $\Delta_g = 64\Delta_{DNS}$ data are also queried, but are not included in the training set and are instead held out as part of the test set to test the neural network generalization capabilities.

Number of Realizations	Filter Width	Domain Size	Flow Type
320	$16\Delta_{DNS}$	16 ³	HIT
320	$16\Delta_{DNS}$	16^{3}	HIT
320	$32\Delta_{DNS}$	8^{3}	HIT
40	$16\Delta_{DNS}$	32^{3}	HIT
40	$32\Delta_{DNS}$	16^{3}	HIT
320	$16\Delta_{DNS}$	16^{3}	Channel
320	$32\Delta_{DNS}$	8^{3}	Channel
40	$16\Delta_{DNS}$	32^{3}	Channel
40	$32\Delta_{DNS}$	16^{3}	Channel

Table 1: Training Data

2.4.2. Loss Function and Metrics

The loss function used for training follows from the loss function introduced in Wu & Lele (2025), involving a two-term loss function that enforces both the root mean squared error between the predicted and actual subgrid stress tensor, as well as the root mean squared error between the predicted and actual energy dissipation, $\epsilon = -\tau_{ij}\bar{S}_{ij}$. As such, the loss function involves:

$$L = \text{RMSE}(\tau_{ii,pred} - \tau_{ii}) / \text{RMS}(\tau_{ii}) + \lambda \text{RMSE}(\epsilon_{pred} - \epsilon) / \text{RMS}(\epsilon)$$
 (2.15)

where λ is a constant that can bias the neural network towards emphasizing the energy dissipation or the predicted values of τ_{ij} . In the present work, following Wu & Lele (2025), $\lambda = 1$ is used, which indicated an equal bias between both loss function terms. The first term of this loss function is termed "RMSE" (unbolded) and the second term of this loss function is termed "DRMSE" (unbolded). Meanwhile, the bolded terms signify the operation of taking the RMSE or RMS of the particular quantity in the parenthesis.

For *a posteriori* tests, both qualitative and quantitative evaluations are important. However, quantitative metrics are often case dependent. Therefore, a few metrics are introduced that can be used to compare the various subgrid stress models with the filtered DNS solution that work for both forced HIT and channel flow. Note that these are necessary but not sufficient metrics to evaluating a subgrid stress model's quality. The first metric involves computing a sum-squared error (SSE) between the filtered DNS spectra and the LES spectra:

$$SSE_{E} = \int_{k} (log(E_{DNS}(k)) - log(E_{LES}(k)))^{2} dk \approx \sum_{k} (log(E_{DNS_{k}}) - log(E_{LES_{k}}))^{2}$$
(2.16)

where the energy spectra is summed over a specific wavenumber band, with k denoting the wavenumber. The logarithm ensures that differences in the spectra at large wavenumbers can still meaningfully increase this metric. Another metric involves computing the the SSE between the filtered DNS and LES correlations (spatial or temporal):

$$SSE_{corr} = \int_{\delta} (C_{DNS}(\delta) - C_{LES}(\delta))^2 d\delta \approx \sum_{\delta} (C_{DNS_{\delta}} - C_{LES_{\delta}})^2$$
 (2.17)

where C denotes the temporal or spatial correlation and δ represents the spacing (temporal or spatial) used to calculate the value of the correlation function. For channel flow, additional

metrics involving the Reynolds Stress profiles can also be developed. One involves computing the SSE over the various Reynolds Stress profiles summed in the wall-normal direction:

$$SSE_{R_{xx}} = \int_{y} (R_{xx_{DNS}}(y) - R_{xx_{LES}}(y))^{2} dy \approx \sum_{y} (R_{xx_{DNSy}} - R_{xx_{LESy}})^{2}$$
 (2.18)

where R_{xx} represents the Reynolds Stress over the "xx" direction (ie 11, 22, 33), while y denotes the wall-normal direction. Another quantitative metric for channel flow involves computing the SSE for the mean velocity profiles, summed over the wall-normal direction:

$$SSE_{u} = \int_{y} (\overline{u(y)}_{DNS} - \overline{u(y)}_{LES})^{2} dy \approx \sum_{y} (\overline{u(y)}_{DNS} - \overline{u(y)}_{LES})^{2}$$
(2.19)

where y once again is the wall-normal direction and u(y) is the LES or filtered DNS mean velocity profile (averaged over the homogenous directions, in this case x and z). The above 4 quantitative metrics do not represent a complete characterization of turbulence, but serve as "first-order" metrics in order to compare various subgrid stress models quantitatively in an a posteriori setting.

3. A priori Results

Here, neural network training hyperparameters are covered, along with information on various other neural network architectures before discussing *a priori* results.

3.1. Neural Network Training Details

All neural networks are trained using the Adam Optimizer using three learning rates of 0.01, 0.001 and 0.0001, and the best performing model is selected. We note that in training all the neural network models, each neural network performed the best using a learning rate of 0.001. In order to facilitate comparisons between the neural network proposed and other neural network models in literature, a TBNN using an artificial neural network frontend was also trained (labeled as "TBNN"), as well as a two neural network Unet architecture introduced by Wu & Lele (2025), which is labeled as "NN". The S4ND model was trained with the bandlimit parameter set to 0.1. For all neural networks, early stopping was employed to ensure that the neural networks do not overfit, with the criteria being that if the validation loss did not decrease for 300 epochs, the neural network weights would be restored to the instance of the lowest validation loss and training would terminate. Table 2 is a table showing the total number of trainable parameters for each neural network model. As seen, all neural networks are roughly the same size, allowing for a fair comparison between the various neural network models.

3.2. Interpolative A Priori Results

For a priori tests, the S4ND model is compared with the ANN-based TBNN, CNN-based TBNN, Static Smagorinsky, and Dynamic Smagorinsky models. First, the spatial distribution of the subgrid stress can be compared for a filter width of $16 \Delta_{DNS}$, which is shown in figure 3.

From figure 3, all the neural network models are far better than the Smagorinsky models in capturing the overall correlation with the filtered DNS subgrid stress, as evidenced by both the higher correlation coefficient and the lower RMSE. The trend among neural networks is also of note, as the simplest neural network (ANN-based TBNN) has the worse RMSE and correlation coefficient out of all the neural network models, yet it has the most trainable

NN Model	Inputs	Trainable Parameters
S4ND	$V_{norm}, S _{norm}, R _{norm}$	9852
NN	Normalized Invariants and Normalized Tensor Basis	12523
TBNN	Normalized Invariants and Normalized Tensor Basis	13210

Table 2: Various Neural Network Model Inputs and Trainable Parameters

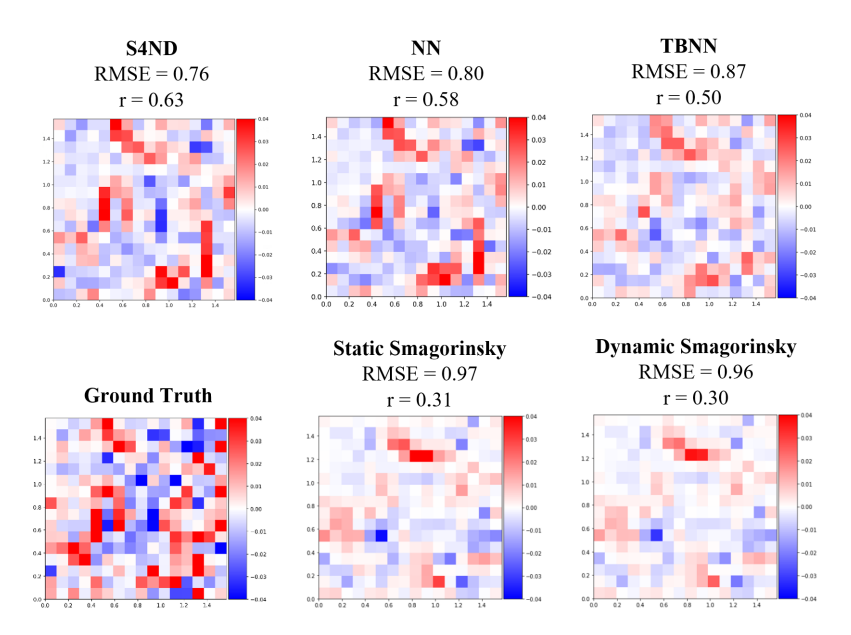


Figure 3: Spatial distribution of τ_{11} for a 2D slice of the 3D domain for a filter width of 16 Δ_{DNS} . All numerical values are ensemble averaged over 10 ensembles, while the spatial fields are chosen randomly for visual reference. The letter r denotes the correlation coefficient. The correlation coefficients are highest for S4ND, while the other, less complex neural networks have lower correlation coefficients.

parameters out of all the neural network models that have been compared. Meanwhile, the more complex neural network models (such as the CNN-based NN model and the S4ND model) perform far better. In addition, the interscale energy transfer field, $\tau_{ij}\bar{S}_{ij}$ is also shown.

Overall, as seen from figure 3 and figure 4, visually, the TBNN field is more diffuse as compared to the S4ND and NN fields, but they are quite similar. In fact, all the fields look relatively similar visually, and the DRMSE are not too far off from one another. This suggests that the neural network models are able to represent the energetics of turbulence faithfully *a priori*, and therefore have a good chance of being stable *a posteriori*, as the interscale energy transfer field is similar to the Static and Dynamic Smagorinsky models, which are known to be stabilizing towards a LES simulation.

In addition, probability density functions (PDFs) showing the overall distribution associated with various models are shown in figure 5a and figure 5b. From figure 4, the overall spatial distribution of $\tau_{ij}\bar{S}_{ij}$ is similar across most models, and this is corroborated when

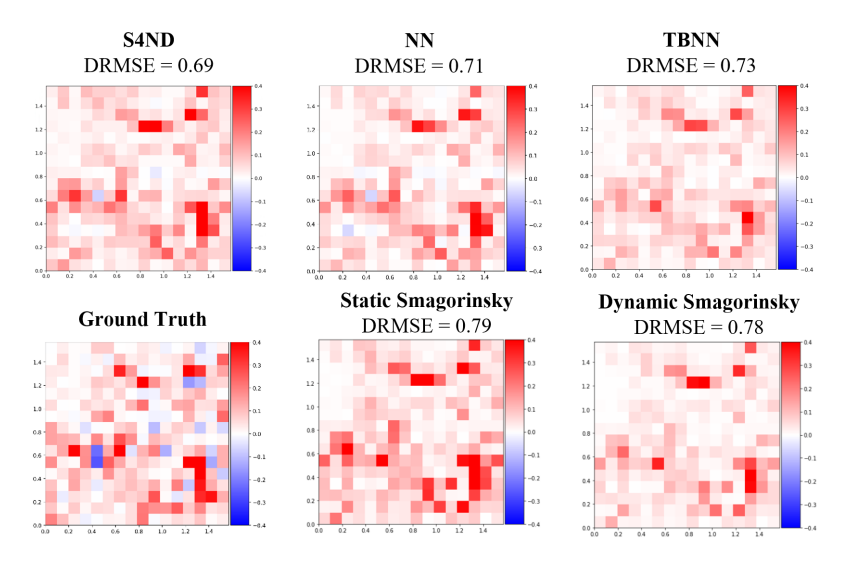


Figure 4: Spatial distribution of $\tau_{ij}\bar{S}_{ij}$ for a 2D slice of the 3D domain for a filter width of 16 Δ_{DNS} . All numerical values are ensemble averaged over 10 ensembles, while the spatial fields are chosen randomly for visual reference.

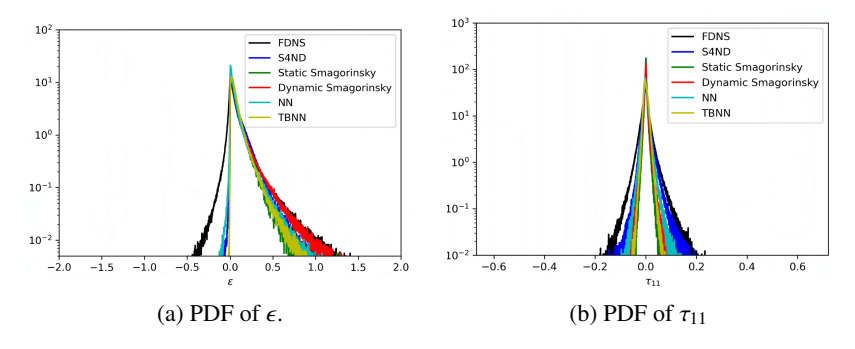


Figure 5: Probability Density Functions for $16~\Delta_{DNS}$ forced HIT. As seen, the S4ND model is more able to accurately capture the distribution of τ_{11} as compared to other models. The S4ND model and NN model (convolution-based) both capture more backscatter than traditional models, although it is still less than FDNS.

evaluating the PDF of ϵ . From figure 5a, one can see that all the models do a good job representing the forward scatter (energy transfer to smaller scales) while they do worse on the back-scatter (energy transfer from small to large scales). However, both the NN and S4ND models have more back-scatter than the traditional models, which barely even have any values smaller than zero. From figure 5b, the overall conclusions drawn from evaluating the spatial distribution are confirmed. Overall,the S4ND model is the closest to the filtered DNS PDF, followed by the CNN-based neural network model (NN), and then followed by the TBNN and the traditional models. Note that in the aggressive filtering regime, the TBNN behaves quite poorly, oftentimes being no better than the Dynamic Smagorinsky model when comparing PDFs. As seen from others in literature, in general, simple ANN-based neural network models can still perform well when compared to traditional models when the filtering is less aggressive (Cho *et al.* 2024; Xie *et al.* 2020b).

From all these results, while adding complexity to the neural network model can help increase performance, as seen since the S4ND and CNN-based models have better perfor-

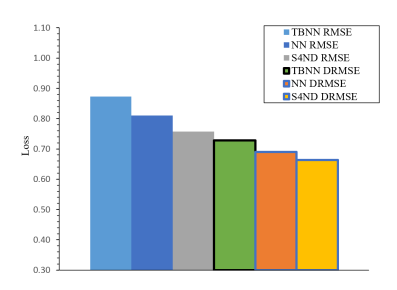


Figure 6: RMSE and DRMSE for various neural network models evaluated on $24\Delta_{DNS}$ HIT data. As seen, the S4ND is able to handle this case the best (no increase in the RMSE and DRMSE as compared to the test set at different other filter widths), followed by the CNN-based model and then the traditional TBNN, which shows a noticeable increase in both the RMSE and DRMSE when compared to the S4ND model.

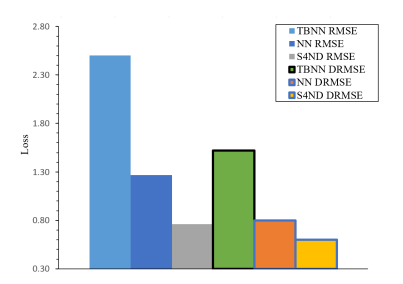


Figure 7: RMSE and DRMSE for various neural network models evaluated on $64\Delta_{DNS}$ HIT data. As seen, the S4ND model is able to extrapolate to this more aggressive filter width without any significant increase in the RMSE and DRMSE, while the CNN-based neural network model has around a factor of 2 increase in the RMSE and a factor of 1.3 in DRMSE. Meanwhile, the traditional TBNN has a loss increase of almost a factor of 4 for RMSE and a loss increase of a factor of 2.5 for DRMSE

mance as compared the the TBNN model, in a setting where the filter width is the same as the training data, it is hard to distinguish between whether the S4ND and CNN-based models are better. This is to be expected, as the continuous convolution kernels that S4ND uses should perform better in extrapolative settings, not necessarily in situations that are part of the training data.

3.3. Extrapolative A Priori Results

While the performance when the filter width is the same as the training set is good, one also needs to evaluate the neural network on different filter widths. First, a less stringent test is applied, where the neural network models, trained on $16\Delta_{DNS}$ and $32\Delta_{DNS}$ data, is evaluated on a filter width of $24\Delta_{DNS}$.

From figure 6, the overall trends hold, where the ANN-based models are the worst-performing, followed then by the CNN-based and then the S4ND models for both RMSE and DRMSE. Overall, all the neural network models are able to extrapolate to this "inbetween" filter width, since the training data consists of $16\Delta_{DNS}$ and $32\Delta_{DNS}$ data. A more challenging case is evaluating the neural network models on $64\Delta_{DNS}$ data, as even more energy is filtered out at this aggressive filter width, meaning that the neural network models must learn scale-similarity in order to extrapolate to this more aggressive filter width. These results are shown in figure 7.

Figure 7 shows that the only neural network model that can successfully extrapolate to

	Table 3:	Filter Widths	and Energy	Filtered	for HIT
--	----------	---------------	------------	----------	---------

Δ_g	Average Energy Filtered	Maximum Observed Energy Filtered		
$1\Delta_{DNS}$	0%	0%		
$2\Delta_{DNS}$	1%	2.1%		
$4\Delta_{DNS}$	2%	5.3%		
$8\Delta_{DNS}$	4%	12.2%		
$16\Delta_{DNS}$	9.6%	23.4%		
$32\Delta_{DNS}$	14.3%	40.4%		
$64\Delta_{DNS}$	22.6%	56.4%		

this filter width is the S4ND model. The ANN-based model does extremely poorly, as the RMSE loss is now multiple times higher than the test set loss at an in-training set filter width, completely failing to generalize. Even the CNN-based model is unable to generalize, as the loss is around twice as high as compared to the in-training set filter width loss. Meanwhile, the S4ND model shows no increase in the loss as compared to filter widths that are within the training set, being the only model that can extrapolate successfully to a setting where the filter width is more aggressive than the training set it was trained on. For reference, Table 3 shows the average turbulent kinetic energy (TKE) filtered out as compared to the reference DNS simulation over multiple ensembles, as well as the maximum TKE filtered out that was observed over the ensembles. As seen, being able to extrapolate to a filter width that is not in the training set, with an average TKE that has been filtered out being 22.6 percent is not an easy task.

4. A Posteriori Results

All neural network models are integrated into an in-house code, PadeOps (Ghate & Lele 2017), to be evaluated in an *a posteriori* setting. In these sections, two traditional models (the Static Smagorinsky and Sigma models) are compared with three neural network models (S4ND, an ANN-based TBNN, and a CNN-based TBNN). These two traditional models were chosen as it represents one of the earliest subgrid stress models and a modern subgrid stress model that has many desirable properties as stated in the introduction. Three neural network models are compared to highlight the benefits gained from increasing the complexity of neural network models.

4.1. *In-training Set Simulation Results*

First, all models are evaluated on LES simulations with grid resolutions corresponding to in-training set filter width cases.

4.1.1. Forced HIT at $16\Delta_{DNS}$

The forced HIT simulation is run with a RK4-5 time stepping scheme (Bogacki & Shampine 1996) on a 64^3 grid, which corresponds to a $16\Delta_{DNS}$ filter width. The spatial discretization scheme is Fourier collocation, possible since the boundary conditions are triply periodic, with a domain length of 2π in each direction. The forcing scheme forces the energy in the wavenumber band below 2 to be constant, and the non-dimensional dissipation, ϵ is set to 0.103 for all simulations. Due to Fourier collocation, $\frac{2}{3}$ dealiasing is applied. For this simulation, all cases have a Taylor Reynolds number (Re_A) of approximately 820. As seen in figure 8, all the LES simulations with various models have reasonable spectra. The eddy viscosity models, as expected, are more dissipative as compared to filtered DNS, while the

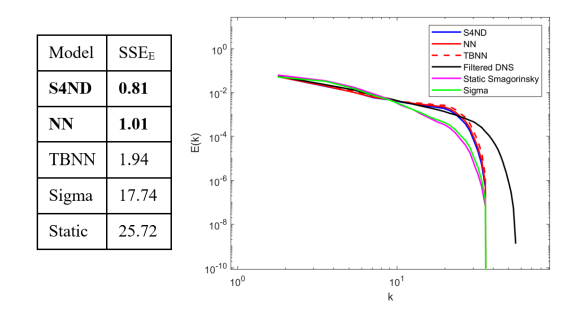


Figure 8: Forced HIT spectra for various SGS models *a posteriori* on a grid size corresponding to a filter width of $16 \Delta_{DNS}$.

neural network models better approximate the overall shape of the spectra but are slightly under-dissipative. From the "bump" in the spectra, the ANN-based subgrid stress model is the most under-dissipative, followed by the CNN-based model, and then the S4ND model. The SSE_E table validates this, as this metric suggests that the S4ND model is the closest to the filtered DNS spectra, as lower SSE_E values are closer to filtered DNS statistical quantities.

From figure 9, all neural network models are fairly good at predicting the temporal decorrelation, as they all follow the overall expected decay shape with the S4ND and ANNbased neural network models being slightly more accurate. When evaluating the spatial correlations, all models are fairly accurate for small spacings, but the S4ND model is less accurate towards the larger spacings compared to both the ANN-based and CNN-based models. While the overall spatial correlation shapes are preserved for all models, as seen from the SSE_{corr} for the spatial decorrelation, the S4ND model has the largest error compared to the filtered DNS decorrelation. From the space-time correlations, one can conclude that all the neural network models are far more accurate than either of the traditional models, especially for small spatial and temporal spacings. It is hard to determine which neural network model is more superior when it comes to space-time correlations. Overall, the benefits of neural network complexity is not clear in this set of simulations, as sometimes the S4ND model is better, while other times (such as when evaluating spatial correlations) it is worse. However, this simulation is run with an in-training set filter width of $16\Delta_{DNS}$, where it has already been established that we do not expect much difference between the S4ND and the CNN-based models. This is reflected in this set of simulations as the S4ND model is sometimes better, and sometimes worse than the CNN-based models. The S4ND model's strength, as seen a priori, is in extrapolative scenarios.

4.1.2. Channel Flow at $16\Delta_{DNS}$

Similarly to the HIT cases, the channel flow simulation is also discretized with Fourier Collocation in the homogeneous directions, while a 6th order compact scheme is used in the wall-normal direction. The wall model used is not data-driven, and instead follows from the wall model used by Bou-Zeid *et al.* (2005). The simulation grid size is 128x96x32, while the domain size is $[8\pi, 3\pi, 2]$, with the streamwise velocity pointing in the "first" direction and the wall-parallel direction being the "second" direction. All simulations run in this section correspond to a filter width of $16\Delta_{DNS}$ with a friction Reynolds number of $Re_{\tau} = 1000$, with $Re_{\tau} = \frac{u_{\tau}H}{\nu}$, where u_{τ} is the friction velocity, H is the channel half-height, and ν is the kinematic viscosity. As seen in figure 10, in a more complex flow (as compared to HIT), the utility of more complicated neural network models is starting to show. The ANN-based TBNN is unable to predict even the spectra properly, and is even worse than

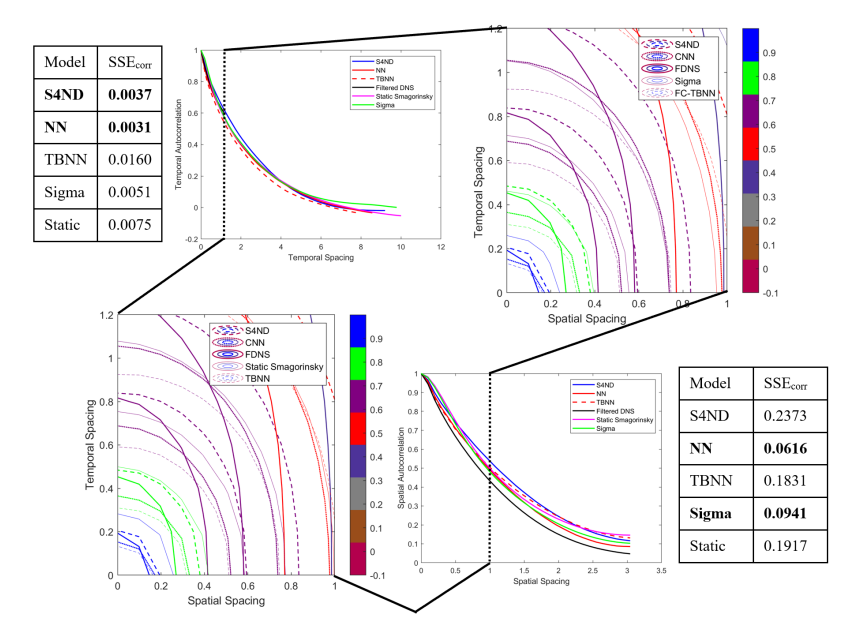


Figure 9: Forced HIT spatial, temporal, and space-time correlations for various SGS models *a posteriori* on a grid size corresponding to a filter width of $16 \Delta_{DNS}$.

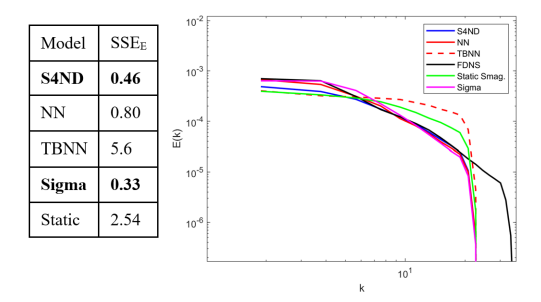


Figure 10: Channel flow spectra at z/H = 0.46875 various SGS models compared to filtered DNS. Both the Static Smagorinsky model and TBNN fail at predicting the overall spectra shape.

Static Smagorinsky. Meanwhile the overall shapes associated with the CNN-based and S4ND model is significantly closer to that of the filtered DNS profile. While the S4ND model is slightly over-dissipative at small scales, it follows the inertial range of the spectra better than the CNN-based model when comparing these two profiles with the filtered DNS profile. Overall, from the SSE_E table, one can see that the S4ND model and the Sigma model are more similar to filtered DNS as compared to the other models.

From figs. 11a to 11b, one can see a similar story when comparing the ANN-based model with its more complex counterparts. The mean profiles associated with the ANN-based TBNN model are inaccurate as compared to filtered DNS, not even predicting the shape properly, while the other two neural network models perform far better. In fact, the spatial correlations associated with the ANN-based TBNN model at aggressive grid spacings highlights that it is completely inaccurate, as the spatial correlations become jagged. Meanwhile, the mean profiles predicted by all the other models that are not the ANN-based TBNN are reasonable,

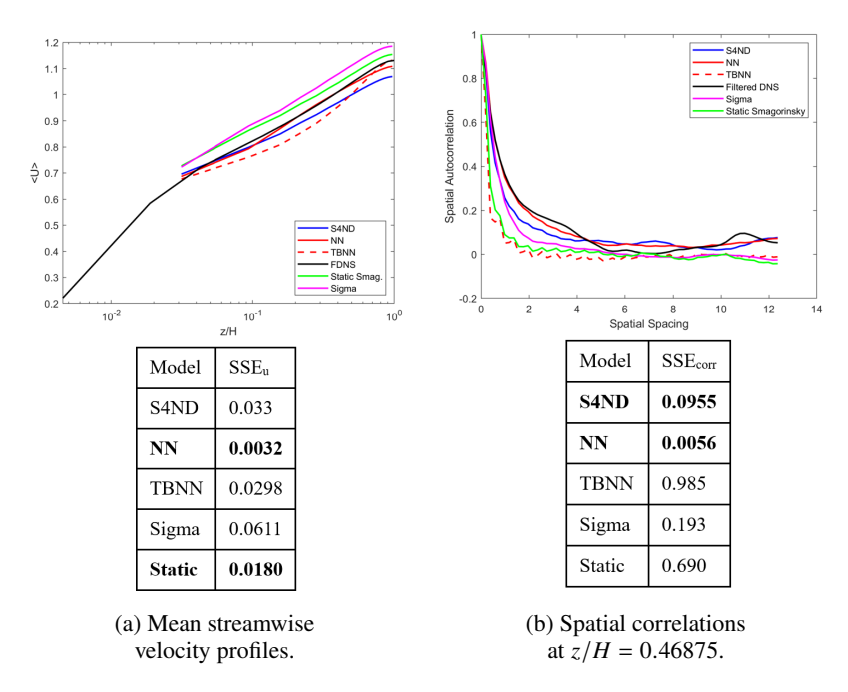


Figure 11: Channel flow macro-scale quantities analyzed for various SGS models. The mean velocity profiles and spatial correlations for the S4ND and NN model look the closest compared to filtered DNS. As seen, the TBNN completely fails in this setting, predicting jagged spatial correlations.

with the CNN-based model being more accurate as compared to the S4ND model. For the spatial correlations, both the S4ND and CNN-based TBNN are far better than the traditional models, with the CNN-based model once again being more accurate.

Reynolds stress profiles are also plotted, which are seen in figs. 12a to 12c. Overall, both the S4ND model and CNN-based model are more accurate compared to the other models, with the S4ND model and CNN-based model trading off in accuracy. When comparing the CNN-based model to the S4ND model, it would seem like for channel flow at this resolution, the CNN-based model is slightly better than the S4ND model. This is seen in the R_{13} profile, as the overall shape of the Reynolds Stress profile is better captured by this model. While the CNN-based model is indeed slightly better than the S4ND model at this resolution, LES grid spacing is ultimately determined by the user, and therefore the models must also be evaluated on an out-of-training set filter width.

4.2. Filter Width Extrapolation Results

Now, all the models are evaluated on an extrapolative filter width that is out of the training set. This will test the generality of the neural network models to see if true "scale-similarity" has been learned. Given that the ANN-based TBNN was completely inaccurate for channel flow already (shown in figure 11b), this section focuses on evaluating the more complex neural network models and comparing them to the traditional models.

4.2.1. Forced HIT at $64\Delta_{DNS}$

Now, fixing all the previous simulation parameters to be identical to the $16\Delta_{DNS}$ HIT simulation except for grid spacing, all models are run on a significantly coarser LES simulation where the number of points is 16^3 , corresponding to a filter width of $64\Delta_{DNS}$. The results are shown in figure 13.

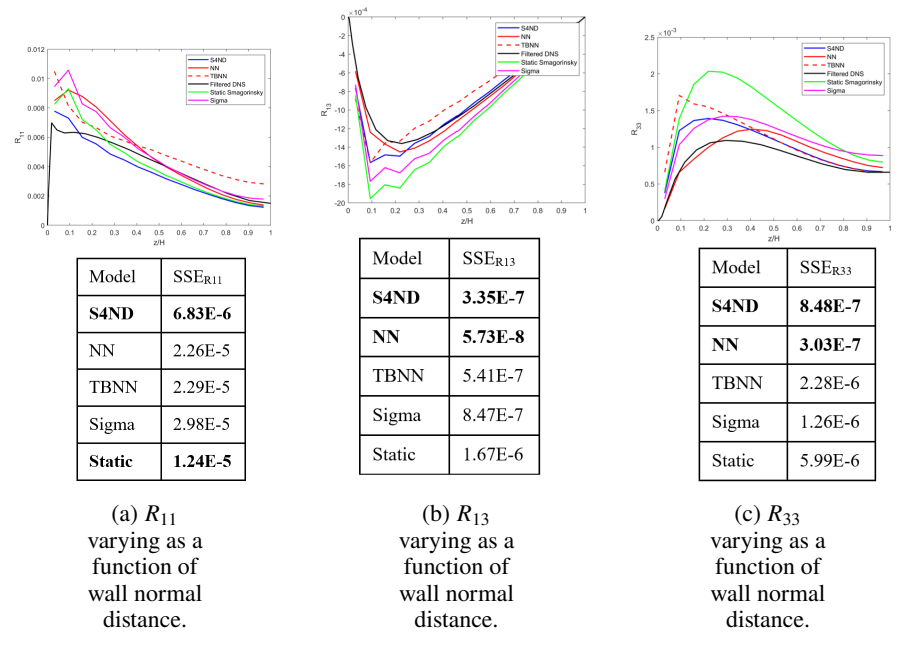


Figure 12: Channel flow Reynolds stress profiles for various SGS models at a filter width corresponding to $16 \Delta_{DNS}$.

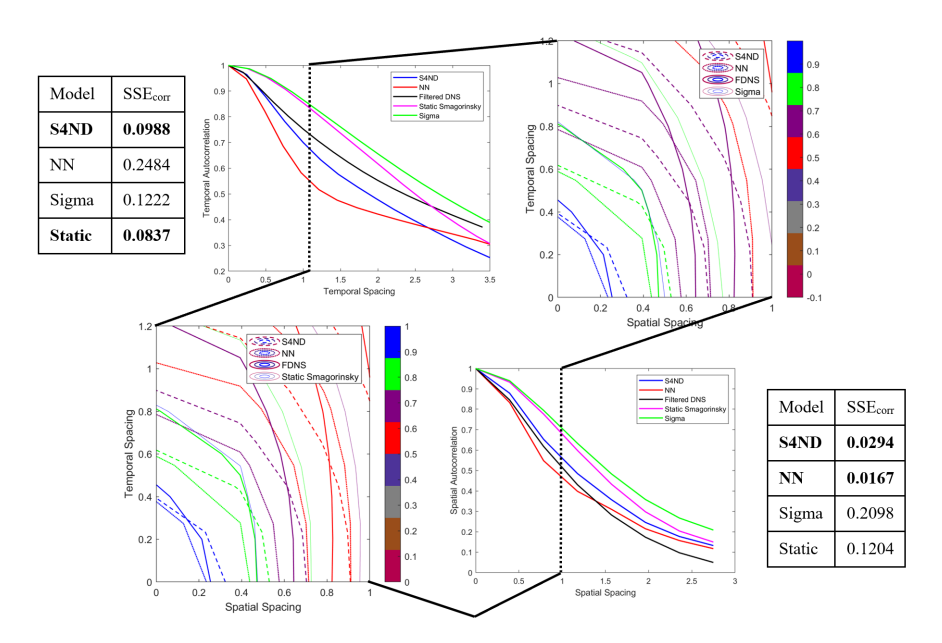


Figure 13: Forced HIT spatial, temporal, and space-time correlations for various SGS models on a grid corresponding to an extrapolative filter width of $64\Delta_{DNS}$.

At this more aggressive grid spacing, the temporal autocorrelations suggest that the S4ND model is far better at extrapolating than the CNN-based model, and outperforms both traditional models. First, the traditional models are unable to predict the initial temporal decay properly, significantly overpredicting the temporal autocorrelation. Meanwhile, the

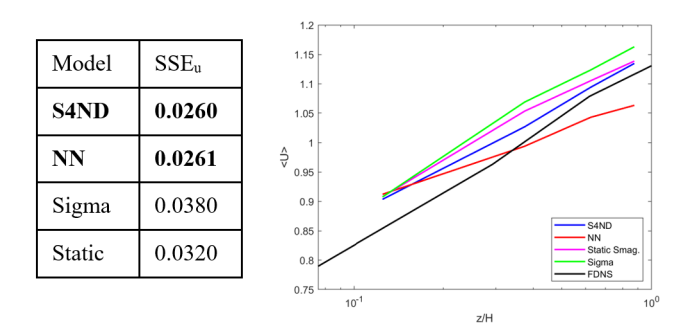


Figure 14: Channel flow mean profiles for various SGS models on a grid corresponding to an extrapolative filter width of $64\Delta_{DNS}$.

CNN-based model decorrelates far too quickly, and then decorrelates far too slowly as the temporal spacing increases. The overall shape of this profile is best approximated by the S4ND model, and this is corroborated by the SSE_{corr} which shows that S4ND has a low SSE_{corr} . However, both quantitative and qualitative analysis must be used, as SSE_{corr} for the Static Smagorinsky model is lower than the S4ND model, but this can be attributed to the Static Smagorinsky model crossing the filtered DNS line and thus the integrated distance between the two curves is smaller due to this crossover. As seen from the temporal decorrelation graph, the overall shape of the Static Smagorinsky correlation is quite different from filtered DNS.

The same story can be seen in the spatial correlations, with one difference being that the CNN-based model now also outperforms the traditional models, and the SSE_{corr} for the CNN-based model is once again artificially lowered due to the line crossing the filtered DNS line. Overall, the S4ND model still preserves the overall shape of the spatial correlations better than all the other models. From the space-time correlations, one can conclude that the traditional models completely fail in predicting the correlations, as the blue lines denote the predicted contour for a particular SGS model. Meanwhile, the traditional model "thin blue contours" in the plots are extremely off, showing a significant underprediction of the decorrelation as compared to both the neural network models. Overall, considering all these factors, the S4ND model is more accurate than the CNN-based model in this setting.

4.2.2. Channel Flow at $64\Delta_{DNS}$

Channel flow is also evaluated at a more aggressive, extrapolative grid spacing. Keeping all other simulation parameters fixed, the grid spacing is changed to 32x24x8, corresponding to a filter width of $64\Delta_{DNS}$. From the mean profiles, shown in figure 14, the S4ND model is able to preserve the slope of the mean streamwise velocity profile as compared to filtered DNS, while the CNN-based model fails. Meanwhile, the two traditional models are more inaccurate as they are further from the filtered DNS profile. This is also seen in the SSE_u tables, with the S4ND being the lowest (and the NN model being not far behind only because it crosses the filtered DNS profile).

The Reynolds Stress profiles are also plotted. From these profiles, the accuracy of the S4ND model in an extrapolative setting is highlighted. Comparing the S4ND model to the CNN-based model, the S4ND model is far more accurate as the CNN-based model has significant trouble extrapolating. The CNN-based model profile shapes are extremely off and the magnitudes are incorrect even when compared to the traditional models. As seen from every single profile, the S4ND is far better at preserving the overall shape and magnitude as compared to both the CNN-based model and all the traditional models. This shows the

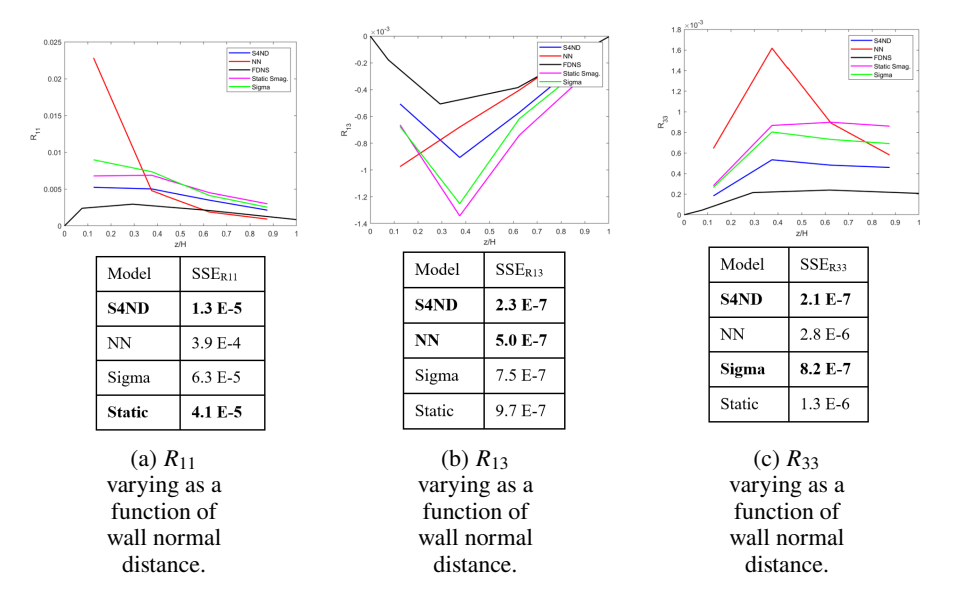


Figure 15: Channel flow Reynolds stress profiles for various SGS models on a grid corresponding to an extrapolative filter width of $64\Delta_{DNS}$.

extrapolatory capability of the S4ND model, as even when extrapolating, it outperforms the CNN-based model while also being significantly better than the traditional models. In all situations, the S4ND-based model, when integrated into a LES simulation, gives results closest to the filtered DNS profiles.

Overall, combined with the HIT results from the previous section, the S4ND model is a more flexible model and more suited to be a SGS model since it is far more accurate in extrapolating than any of the other neural network models tested, and is more accurate than the traditional SGS models even when extrapolating. While the in training set filter width *a posteriori* results are slightly less accurate than the CNN-based model, it trades that slight accuracy decrease for better extrapolatory capability (in grid spacing) than the CNN-based model.

5. Reynolds Number Scaling

The Reynolds number scaling capabilities of the S4ND model are now investigated. First, the S4ND model, which is trained on forced HIT with $Re_{\lambda} = 820$ and channel flow with $Re_{\tau} = 1000$ data, is tested *a posteriori* on both forced HIT with $Re_{\lambda} = 2400$ and channel flow with $Re_{\tau} = 5200$. Next, the S4ND model is then tested on cases where not only the grid width, but the Reynolds Number is also extrapolated.

5.1. Reynolds Number Scaling with DNS Data

Both HIT and channel flow Reynolds number scaling is investigated. The HIT simulation is conducted on a 64^3 grid on a triply periodic domain of length 2π in each direction, with the dimensional dissipation, ϵ , set to 1.4144. The channel flow simulation is conducted on a grid of size $128 \times 32 \times 96$ on a domain of size $8\pi \times 2 \times 3\pi$. Due to the increase in Reynolds number, while the $\Delta_{LES} = 64\Delta_{DNS}$ for HIT and $\Delta_{LES} = 80\Delta_{DNS}$ for the channel flow simulation, the overall grid spacing is still considered in training set. This is because the grid spacing dx, dy, dz are grid spacings that the neural network has been trained on in the

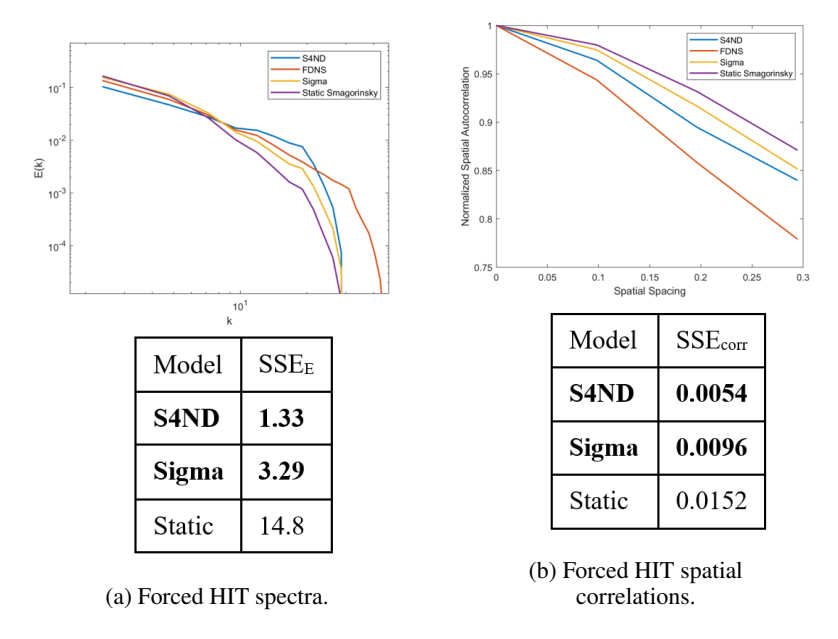


Figure 16: Macro-scale quantities analyzed for forced HIT at a higher Reynolds number not seen in the training set.

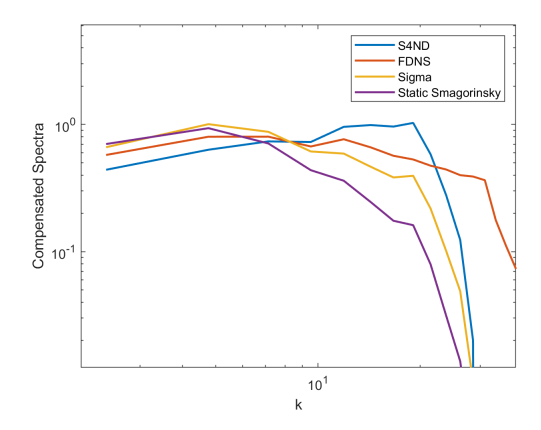


Figure 17: Compensated Spectra for forced HIT at a higher Reynolds number not seen in the training set.

training data. As seen from Cho *et al.* (2024), neural networks extrapolate well to higher Reynolds number as long as dx, dy, dz is the same as the grid spacing of the training data, even if $\frac{\Delta_{LES}}{\eta}$ is larger than the training data, where η is the Kolmogorov length scale. As such, we will still consider this a "in training set" filter width.

5.1.1. HIT

The Reynolds number scaling results for forced HIT are shown in figures 16a and 16b. In these figures, the S4ND model is compared to both the Static Smagorinsky and Sigma models, as well as filtered DNS to evaluate the extrapolatory capability of the S4ND model.

As seen, when the Reynolds number is larger than the training set Reynolds number, the S4ND model still produces reasonable results for both spectra and spatial correlations.

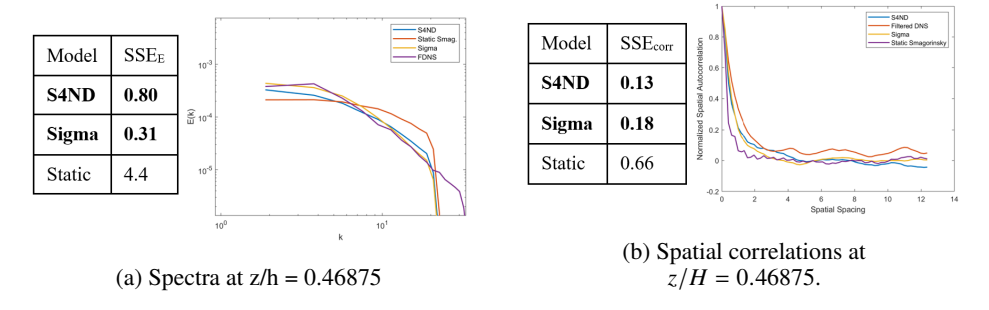


Figure 18: Macro-scale quantities analyzed for channel flow at a higher Reynolds number not seen in the training set.

Overall, the same trends hold when comparing the S4ND simulations that were run with an in-training set Reynolds number versus an extrapolatory Reynolds number. For example, the energy spectra for S4ND is still slightly underdissipative, while the spatial correlations are more accurate for the S4ND model compared to the spatial correlations produced by the traditional subgrid stress models. In this case, the spatial correlations are truncated since there is only one ensemble at this Reynolds number for the filtered DNS profile (JHTDB provides one snapshot), and thus the spatial correlation is truncated at a point where it is still reasonably converged. When taking a look at the SSE for both the energy spectra and the correlations, the S4ND model has the lowest error out of all the models compared. The compensated spectra, which pre-multiplies the energy spectra with a $k^{\frac{5}{3}}$ factor, is shown in figure 17. As seen, the filtered DNS reference has an inertial range, but the inertial range varies from being slightly less than the $k^{\frac{5}{3}}$ scaling to slightly more than the $k^{\frac{5}{3}}$ scaling. This is also seen in the SGS models, with the S4ND model being consistent with previous results (slightly under-dissipative) while the traditional SGS models are also consistent with previous results (slight over-dissipative). Overall, the S4ND model is able to successfully extrapolate to a higher Reynolds number for forced HIT.

5.1.2. Channel Flow

For channel flow Reynolds number scaling, first the spectra at a specific wall normal location and the spatial correlations are shown in figures 18a and 18b. As seen in the plots, the S4ND model produces spectra and spatial correlations that match filtered DNS profiles when the Reynolds number is out of the training set. There is no obvious performance degredation when compared to the in-training set filter width, and the overall profiles match the filtered DNS profiles. Furthermore, the S4ND Reynolds stress profiles are seen in figures 19a, 19b and 19c. Overall, the S4ND model is able to capture the overall shape and magnitude of the Reynolds stress profiles associated with channel flow. From all these plots, the S4ND model is in general, consistent with the in-training set Reynolds number, with no obvious performance degradation when the Reynolds number is out of the training set. This is corroborated by looking at the SSE, where the S4ND model is always top two in SSE for all quantities, which can't be said for the other traditional models. Combining both the channel flow and forced HIT results, one can conclude that the S4ND model is able to extrapolate to higher Reynolds number flow cases and still match filtered DNS reasonably well.

5.2. Extreme Reynolds Number Scaling Without DNS Data

Now, true "out of training set" filter width and Reynolds number extrapolation is run, where the grid spacings dx, dy, dz are larger than the training set, and where $\frac{\Delta_{LES}}{n}$ is also far larger

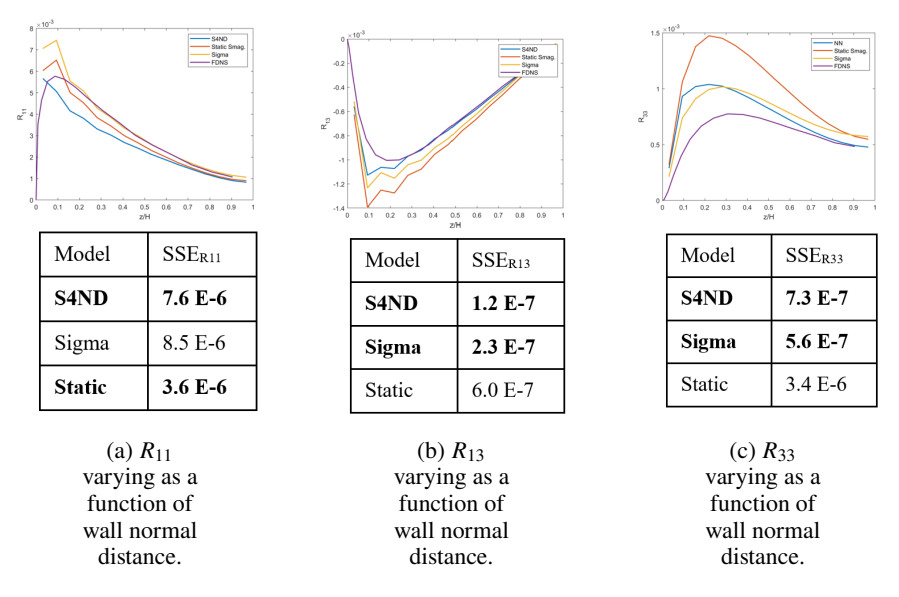


Figure 19: Channel flow Reynolds stress profiles for various SGS models at a higher Reynolds number not seen in the training set.

than the training set. While there are no DNS results at these larger Reynolds numbers, one can evaluate the stability of the subgrid stress models in extreme Reynolds number scaling scenarios.

5.2.1. HIT

The HIT simulation is evaluated on a 16^3 grid, corresponding to a grid spacing in each direction that is twice as large as the training set. Furthermore, 5 Reynolds numbers based on the Taylor microscale are tested: $Re_1 = 4800$, $Re_2 = 19500$, $Re_3 = 56900$, $Re_4 = 515000$, $Re_5 = 508900000$. The S4ND model is only trained on Re = 820. As seen in figures 20a and 20b, the neural network is able to ensure that the LES simulation is stable, even when extrapolating in both grid spacing and Re. Overall, the spectra and spatial correlations look reasonable for all Re, showing that the S4ND model produces reasonable results even if the Reynolds number is over 600000 times that of the training set. Given the coarseness of the grid, the results should not change drastically with Reynolds number, which is demonstrated in these plots. In addition, up to Re_3 , the trends are monotonic, suggesting that the S4ND model can capture trends up to around 70 times the Reynolds number in the training set. From Re_1 to Re_5 , at no point is a "tail-up" in the spectra seen, which is expected for ANN-based subgrid stress models that are trained on only one Reynolds number, as seen in Cho et al. (2024).

5.2.2. Channel Flow

The same neural network is also integrated into a channel flow simulation with varying Reynolds numbers to test the extrapolatory capabilities of the neural network, on a grid of size $32 \times 8 \times 24$ on a domain of size $8\pi \times 2 \times 3\pi$ (grid spacing is coarser than the training set). The Reynolds number based on friction velocity tested involve $Re_1 = 5,200$, $Re_2 = 20,000$, $Re_3 = 50,000$, $Re_4 = 500,000$, and $Re_5 = 500,000$, 000. The neural network is trained only on Reynolds number based on friction velocity of Re = 1000.

From figure 21a, when scaled with friction velocity, the channel mean streamwise velocity profiles collapse nicely, suggesting that these profiles are reasonable for all Reynolds numbers.

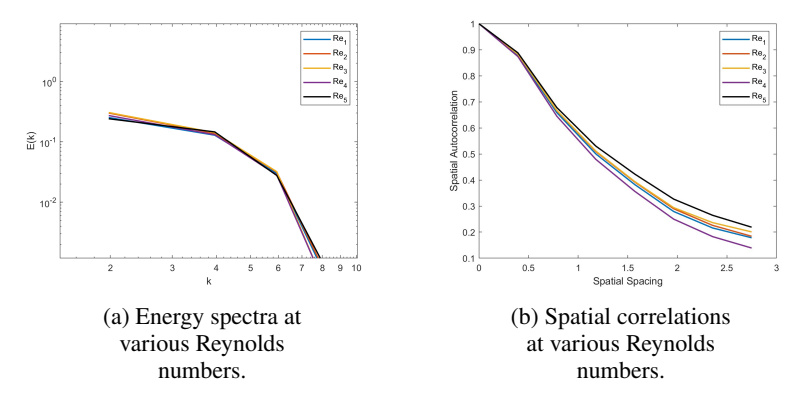


Figure 20: Extreme Reynolds number scaling for HIT

To fully verify this, the log-law profiles are plotted, along with the Sigma model mean profile results in figure 21b. Due to the large offset from the S4ND model, the Sigma model was also run as verification to isolate if this offset was associated with the subgrid stress model or the wall model. As seen, using the classic offset of B = 5.0 is insufficient, likely due to the error in the wall model. This error can be attributed to the wall model since two different SGS models (Sigma model and data-driven S4ND model) produce extremely similar results at the first off-wall grid point, which is dominated by the wall model error. In this extremely coarse and extremely aggressive Reynolds number extrapolation case, the S4ND model is able to produce a profile that is closer to the log-law profile than the Sigma model. From all this, the neural network is seen to provide reasonable results even when the Reynolds number is extrapolated by over 500000 times the Reynolds number of the training set when considering mean profiles. This is further corroborated in figures 22a, 22b, and 22c, where the Reynolds stresses also collapse reasonably well when scaled with friction velocity. There is no significant performance degradation visible at first glance as the Reynolds number increases, suggesting that the S4ND model remains stable even at Reynolds numbers significantly larger than the training set Reynolds number. While exact comparisons can not be made as there is no DNS at these higher Reynolds number cases $(Re_2 - Re_5)$, if the neural network is unable to extrapolate, as seen in Cho et al. (2024), the change in shape of the profiles of turbulent statistical quantities is quite obvious to see.

In order to provide first-order analysis on the reasonableness of the channel flow scaling results, the implied skin friction coefficient, C_f is plotted, as well as the expected inverse log(Re) scaling that is supported by Schultz & Flack (2013). These results are shown in figure 23. As seen, the implied C_f is decreasing for the first 4 Reynolds numbers, and is still reasonably following the overall trend. However, the last Reynolds number suggests an increase in C_f , suggesting that the results are less trustworthy at the highest Reynolds number. However, it is very likely this is more of a wall modelling error as compared to a subgrid stress model error, as in these really coarse simulations there are 8 points across the channel and the wall model's accuracy is suspect at these extreme Reynolds number cases $(Re_{\tau} \text{ of } 500,000,000)$. This argument is further enhanced when the Sigma model results are taken into account, as it exhibits similar trends as compared to the S4ND model. Therefore, the S4ND model likely extrapolates well to these extremely out of training set Reynolds numbers, and the error that is seen can be attributed to the non-data driven wall model. Even if this largest Reynolds number data point is discarded, obtaining 500x friction Reynolds number scaling when the model is only trained on one friction Reynolds number is still excellent. The largest Reynolds number data point is mainly kept to show that even if the

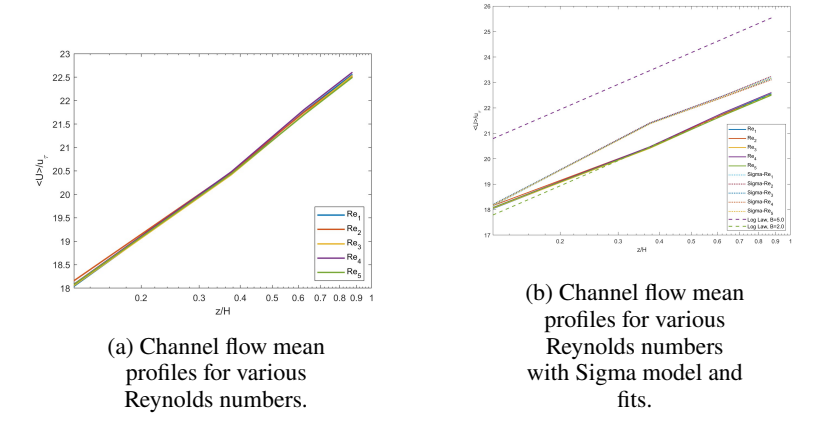


Figure 21: Various mean profiles for channel flow extrapolation to extreme Reynolds numbers.

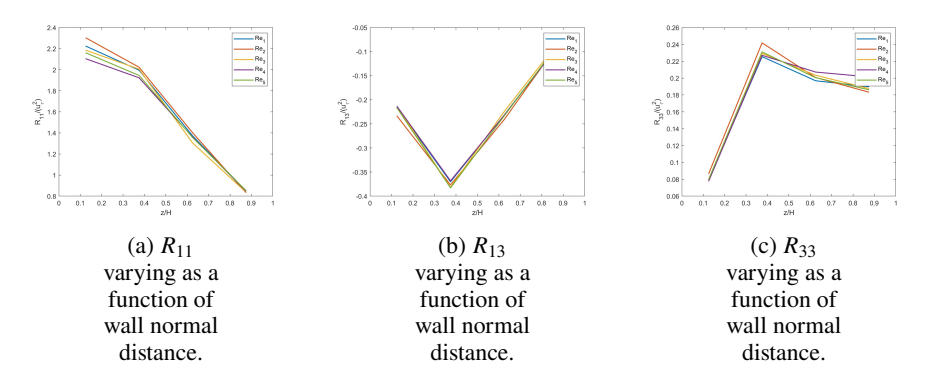


Figure 22: Reynolds stress profiles for various extreme Reynolds numbers for the S4ND model.

results are less trustworthy, the subgrid stress model still remains stable even in this sort of highly extrapolatory situation.

To our knowledge, this is the first demonstration of successful extrapolation in both Reynolds number and filter width for two different flows using the same neural network with no training data augmentation in the coarse grid regime.

5.3. Computational Cost

The computational cost of various models are listed, normalized by the Static Smagorinsky computation time. In general, using TBNNs are more expensive due to the computation of the invariants and the tensor basis, which are the dominant computational costs of the model, as seen in figure 24. Overall, the actual cost to evaluate the neural network models is cheaper than a Dynamic Smagorinsky evaluation, but the computation of the invariants and associated tensor basis significantly dominate the time. Overall, the neural network models are around 3-4 times more expensive than a Dynamic Smagorinsky evaluation. Due to the use of the velocity gradient tensor instead of the invariants, the S4ND model is less costly than the ANN-based TBNN (FC TBNN) and the CNN-based model (Two NN Model). However, even with the increase in computation cost, the simulations are still fairly computationally

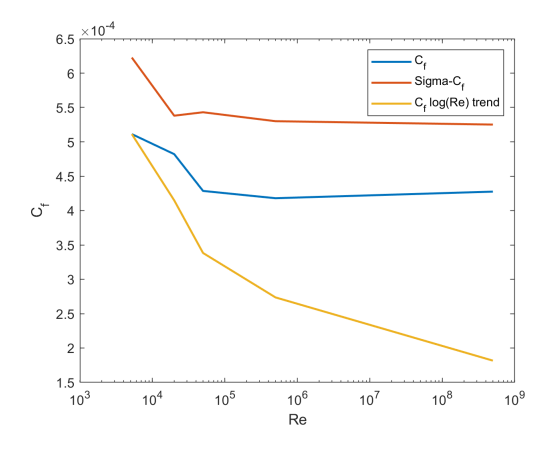


Figure 23: Implied wall skin friction coefficient versus a first-order trend, with the x-axis being friction Reynolds number. The trends show that the error is likely due to the wall model, as both the S4ND model (plotted in blue) and the Sigma model (plotted in red) show similar trends and deviation from the expected trend (plotted in yellow).

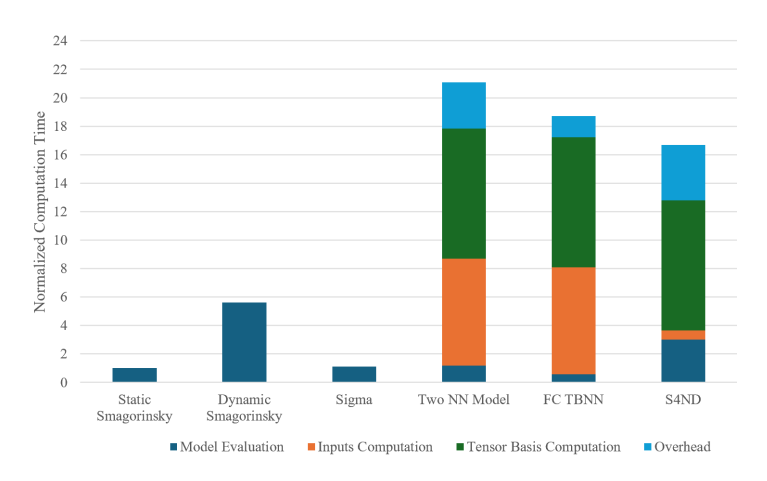


Figure 24: Computational cost of various subgrid stress models. Overhead refers to the time it takes to load the neural network from disk and send the inputs from the LES simulation to the neural network for computation, and then returning the neural network subgrid stress output back to the LES simulation.

inexpensive, requiring less than a day to complete even when evaluating the most expensive neural network models.

6. Conclusions

A new neural network subgrid stress model based on state space sequence models (S4ND) was introduced, and bandlimiting was used to increase the generalization capabilities of the model to untrained grid spacings. A priori, the use of bandlimiting does not restrict the expressivity of the learned representation as compared to other traditional and neural network models, while learning a continuous convolution kernel and using bandlimiting allows the neural network to generalize to more aggressive, untrained grid spacings. A posteriori, when testing on untrained grid widths, the S4ND model is far more accurate than traditional models and is able to generalize where other neural network models fail on both forced HIT and channel flow LES simulations. In addition, even when extrapolating in grid width and Reynolds number at the same time, the S4ND model is stable for both forced HIT and channel flow even when evaluated on Reynolds numbers that are over 500000 times larger than the training set Reynolds numbers, achieving true one-shot Reynolds number extrapolation capability.

Acknowledgements. This work used CPU and GPU resources via Darwin at the University of Delaware and via Bridges2 at the Pittsburgh Supercomputing Center through allocation PHY230025 from the Advanced Cyberinfrastructure Coordination Ecosystem: Services & Support (ACCESS) program, which is supported by National Science Foundation grants #2138259, #2138286, #2138307, #2137603, and #2138296. DNS data is provided by the Johns Hopkins Turbulence Database.

Funding. Andy Wu is partially supported by NASA Cooperative Agreement number 80NSSC22M0108 and Northrop Grumman, as well as the NDSEG Fellowship.

Declaration of Interests. Declaration of Interests. The authors report no conflict of interest.

Data Availability Statement. All DNS data that was filtered to produce the training data for the neural network is provided publicly on JHTDB. A public repository of the S4ND model used can be found in the references section, linking to the author's implementation. Any of the LES simulation data done by the authors is available upon request.

REFERENCES

- BAE, H JANE & KOUMOUTSAKOS, PETROS 2022 Scientific multi-agent reinforcement learning for wall-models of turbulent flows. *Nature Communications* 13 (1), 1443.
- Bardina, Jorge 1983 Improved turbulence models based on large eddy simulation of homogeneous, incompressible, turbulent flows. Stanford University.
- Beck, A, Flad, D & Munz, C-D 2019 Deep neural networks for data-driven LES closure models. *Journal of Computational Physics* **398** (108910).
- ВЕСК, A & Kurz, M 2021 A Perspective on Machine Learning Methods in Turbulence Modelling. Surveys for Applied Mathematics and Mechanics 44 (1).
- Berselli, LC, Iliescu, T & Layton, W J 2006 Mathematics of Large Eddy Simulation of Turbulent Flows, 1st edn. Springer.
- BOGACKI, P. & SHAMPINE, L.F. 1996 An efficient Runge-Kutta (4,5) pair. *Computers & Mathematics with Applications* **32** (6), 15–28.
- Bou-Zeid, Elie, Meneveau, Charles & Parlange, Marc 2005 A scale-dependent Lagrangian dynamic model for large eddy simulation of complex turbulent flows. *Physics of fluids* 17 (2).
- Cheng, Yu, Giometto, Marco G, Kauffmann, Pit, Lin, Ling, Cao, Chen, Zupnick, Cody, Li, Harold, Li, Qi, Huang, Yu, Abernathey, Ryan & others 2022 Deep learning for subgrid-scale turbulence modeling in large-eddy simulations of the convective atmospheric boundary layer. *Journal of Advances in Modeling Earth Systems* 14 (5), e2021MS002847.
- Сно, Сномбнүйк, Ракк, Jonghwan & Choi, Haecheon 2024 A recursive neural-network-based subgridscale model for large eddy simulation: application to homogeneous isotropic turbulence. *Journal of Fluid Mechanics* 1000, A76.
- CLARK, ROBERT A, FERZIGER, JOEL H & REYNOLDS, WILLIAM CRAIG 1979 Evaluation of subgrid-scale models using an accurately simulated turbulent flow. *Journal of fluid mechanics* 91 (1), 1–16.

- GERMANO, MASSIMO, PIOMELLI, UGO, MOIN, PARVIZ & CABOT, WILLIAM H 1991 A dynamic subgrid-scale eddy viscosity model. *Physics of Fluids A: Fluid Dynamics* **3** (7), 1760–1765.
- GHATE, A S & LELE, S K 2017 Subfilter-scale Enrichment of Planetary Boundary Layer Large Eddy Simulation Using Discrete Fourier–Gabor modes. *Journal of Fluid Mechanics* 819.
- GOC, KONRAD A, LEHMKUHL, ORIOL, PARK, GEORGE ILHWAN, BOSE, SANJEEB T & MOIN, PARVIZ 2021 Large eddy simulation of aircraft at affordable cost: a milestone in computational fluid dynamics. Flow 1, E14.
- Graham, Jason, Kanov, K, Yang, XIA, Lee, M, Malaya, N, Lalescu, CC, Burns, R, Eyink, G, Szalay, A, Moser, RD & others 2016 A web services accessible database of turbulent channel flow and its use for testing a new integral wall model for les. *Journal of Turbulence* 17 (2), 181–215.
- Gu, Albert, Goel, Karan & Ré, Christopher 2021 Efficiently modeling long sequences with structured state spaces. arXiv preprint arXiv:2111.00396.
- Guan, Yifei, Chattopadhyay, Ashesh, Subel, Adam & Hassanzadeh, Pedram 2022 Stable a posteriori LES of 2d turbulence using convolutional neural networks: Backscattering analysis and generalization to higher re via transfer learning. *Journal of Computational Physics* **458**, 111090.
- Kang, M, Jeon, Y & You, D 2023 Neural-network-based mixed subgrid-scale model for turbulent flow. *Journal of Fluid Mechanics* **962**.
- Kurz, Marius, Offenhäuser, Philipp & Beck, Andrea 2023 Deep reinforcement learning for turbulence modeling in large eddy simulations. *International Journal of Heat and Fluid Flow* **99**, 109094.
- LI, Y, PERLMAN, E, WAN, M, YANG, Y, MENEVEAU, C, BURNS, R, CHEN, S, A, SZALAY & EYINK, G 2008
 A public turbulence database cluster and applications to study Lagrangian evolution of velocity increments in turbulence. *Journal of Turbulence* 9 (31).
- LI, ZONGYI, KOVACHKI, NIKOLA, AZIZZADENESHELI, KAMYAR, LIU, BURIGEDE, BHATTACHARYA, KAUSHIK, STUART, ANDREW & ANANDKUMAR, ANIMA 2021 Fourier neural operator for parametric partial differential equations, arXiv: 2010.08895.
- Ling, J, Kurzawski, A & Templeton, J 2016 Reynolds averaged turbulence modelling using deep neural networks with embedded invariance. *Journal of Fluid Mechanics* **807**, 155–166.
- MAEJIMAM, SOJU & KAWAI, SOSHI 2024 Coarse-grid large-eddy simulation by unsupervised-learning-based sub-grid scale modeling. In *AIAA SciTech 2024 Forum*, pp. AIAA 2024–1361.
- NGUYEN, ERIC, GOEL, KARAN, GU, ALBERT, DOWNS, GORDON, SHAH, PREEY, DAO, TRI, BACCUS, STEPHEN & RÉ, CHRISTOPHER 2022 S4nd: Modeling images and videos as multidimensional signals with state spaces. *Advances in neural information processing systems* **35**, 2846–2861.
- NICOUD, FRANCK, TODA, HUBERT BAYA, CABRIT, OLIVIER, BOSE, SANJEEB & LEE, JUNGIL 2011 Using singular values to build a subgrid-scale model for large eddy simulations. *Physics of fluids* **23** (8).
- Park, J & Choi, H 2021 Toward neural-network-based large eddy simulation: application to turbulent channel flow. *Journal of Fluid Mechanics* **914**.
- Pawar, Suraj, San, Omer, Rasheed, Adil & Vedula, Prakash 2020 A priori analysis on deep learning of subgrid-scale parameterizations for Kraichnan turbulence. *Theoretical and Computational Fluid Dynamics* **34** (4), 429–455.
- Perlman, E, Burns, R, Li, Y & Meneveau, C 2007 Data Exploration of Turbulence Simulations using a Database Cluster. In *Supercomputing SC07, ACM*. IEEE.
- POPE, S B 2000 Turbulent Flows, 1st edn. Cambridge University.
- Prakash, P, Jansen, K E & Evans, J A 2022 Invariant data-driven subgrid stress modeling in the strain-rate eigenframe for large eddy simulation. *Computer Methods in Applied Mechanics and Engineering* **399** (115457).
- ROBERTS, RICHARD A & MULLIS, CLIFFORD T 1987 Digital signal processing. Addison-Wesley Longman Publishing Co., Inc.
- SAGAUT, P 2006 Large Eddy Simulation for Incompressible Flows: An Introduction, 3rd edn. Springer Science & Business Media.
- Sarghini, F, De Felice, G & Santini, S 2003 Neural networks based subgrid scale modeling in large eddy simulations. *Computers & Fluids* **32** (1), 97–108.
- Schultz, Michael P & Flack, Karen A 2013 Reynolds-number scaling of turbulent channel flow. *Physics of Fluids* **25** (2).
- Scotti, A, Meneveau, C & Lilly, DK 1993 Generalized Smagorinsky model for anisotropic grids. *Physics of Fluids* 5.
- SIRIGNANO, JUSTIN & MACART, JONATHAN F 2023 Deep learning closure models for large-eddy simulation of flows around bluff bodies. *Journal of Fluid Mechanics* **966**, A26.

- SMAGORINSKY, JOSEPH 1963 General circulation experiments with the primitive equations: I. the basic experiment. *Monthly weather review* **91** (3), 99–164.
- STALLCUP, E W, KSHITIJ, A & DAHM, W J 2022 Adaptive Scale-Similar Closure for Large Eddy Simulations. Part 1: Subgrid Stress Closure. In *AIAA SciTech*, pp. AIAA 2022–0595. San Diego, CA: AIAA.
- Stoffer, R, Leeuwen, C M, Podareanu, D, Codreanu, V, Veerman, M A, Janssens, M, Hartogensis, O K & Heerwaarden, C C 2021 Development of a large-eddy simulation subgrid model based on artificial neural networks: a case study of turbulent channel flow. *Geoscientific Model Development* 14 (6).
- STOLZ, STEFFEN, ADAMS, NIKOLAUS A & KLEISER, LEONHARD 2001 An approximate deconvolution model for large-eddy simulation with application to incompressible wall-bounded flows. *Physics of fluids* **13** (4), 997–1015.
- VREMAN, A W 2004 An eddy-viscosity subgrid-scale model for turbulent shear flow: Algebraic theory and applications. *Physics of Fluids* **16** (10).
- Wang, Zhuo, Luo, Kun, Li, Dong, Tan, Junhua & Fan, Jianren 2018 Investigations of data-driven closure for subgrid-scale stress in large-eddy simulation. *Physics of Fluids* **30** (12).
- Wu, Andy 2025 S4ND_SGS_Model.https://github.com/awu1018/S4ND_SGS_Model/tree/main.
- Wu, Andy & Lele, Sanjiva K 2025 Two neural network unet architecture for subfilter stress modeling. *Physical Review Fluids* **10** (1), 014601.
- XIE, C, Wang, J & Weinan, E 2020a Modeling subgrid-scale forces by spatial artificial neural networks in large eddy simulation of turbulence. *Physical Review of Fluids* 5 (5).
- XIE, C, Yuan, Z & Wang, J 2020b Artificial neural network-based nonlinear algebraic models for large eddy simulation of turbulence. *Physical of Fluids* **32** (11).
- Yuan, Zelong, Wang, Yunpeng, Xie, Chenyue & Wang, Jianchun 2021 Dynamic iterative approximate deconvolution models for large-eddy simulation of turbulence. *Physics of Fluids* 33 (8).
- Yuan, Zelong, Xie, Chenyue & Wang, Jianchun 2020 Deconvolutional artificial neural network models for large eddy simulation of turbulence. *Physics of Fluids* **32** (11).